Published in final edited form as:
Arch Oral Biol. 2012 December ; 57(12): 1585–1594. doi:10.1016/j.archoralbio.2012.04.014.

IDENTIFICATION OF A PROTEIN-CONTAINING ENAMEL MATRIX LAYER WHICH BRIDGES WITH THE DENTIN-ENAMEL JUNCTION OF ADULT HUMAN TEETH[1]

Vladimir Dusevich, **Changqi Xu**, **Yong Wang**, **Mary P. Walker**, and **Jeff P. Gorski**[*]
Department of Oral Biology, School of Dentistry, University of Missouri-Kansas City, Kansas City, MO 64108

Abstract

Objective—To investigate the ultrastructure and chemical composition of the dentin-enamel junction and adjacent enamel of minimally processed third molar tooth sections.

Design—Undecalcified human third molar erupted teeth were sectioned and etched with 4% EDTA or 37% phosphoric acid prior to visualization by scanning electron microscopy. Confocal Raman spectroscopy was carried out at 50 μm and more than 400 μm away from the dentin-enamel junction before and after mild etching.

Results—A novel organic protein-containing enamel matrix layer was identified for the first time using scanning electron microscopy of etched bucco-lingual sections of crowns. This layer resembles a three-dimensional fibrous meshwork that is visually distinct from enamel “tufts”. Previous studies have generally used harsher solvent conditions which likely removed this layer and precluded its prior characterization. The shape of the organic enamel layer generally reflected that of sheath regions of enamel rods and extended from the dentin-enamel junction about 100–400 μm into the cuspal enamel. This layer exhibited a Raman C—H stretching peak at ~2931 cm^{-1} characteristic of proteins and this signal correlated directly with the presence and location of the matrix layer as identified by scanning electron microscopy.

Conclusions—The enamel protein layer was most prominent close to the dentin-enamel junction and was largely absent in cuspal enamel >400 μm away from the dentin enamel junction. We hypothesize that this protein containing matrix layer could provide an important biomechanical linkage between the enamel and the dentin-enamel junction and by extension, with the dentin, of the adult tooth.

Keywords

dentin-enamel junction; interphase organic matrix; prism sheaths; Raman spectroscopy; etching; adult teeth; scanning electron microscopy

[1]Footnote to the title: supported by NIH/NIDCR R01DE021462.

[*]**Address correspondence to**: Jeff P. Gorski, Department of Oral Biology, School of Dentistry, Univ. of Missouri-Kansas City, 650 East 25th street, Kansas City, MO 64108. gorskij@umkc.edu. **Phone**: 816-235-2537. **Fax**: 816-235-5524.

INTRODUCTION

Developing enamel extracellular matrix initially contains no mineral crystals but is enriched in amelogenin, the predominant protein component of secretory stage enamel, along with enamelin. MMP-20[2] is believed responsible for catalyzing required processing of amelogenins needed to initiate mineralization of the enamel (1, 2). As the enamel matures, amelogenin is largely degraded by kallikrein-4 yielding mature mineralized enamel containing low contents of enamelin, ameloblastin, and an amelogenin fragment (3–5). As a result, the most mature enamel in the mouse is estimated to contain only 25–30% the maximal protein content of developing enamel (6).

Mature enamel is a brittle material composed predominantly of carbonated calcium hydroxyapatite (96%) with 3% water and ~1% organic matrix (7). In contrast, tooth dentin is a collagenous tissue which is traversed by dentinal tubules which contain cytoplasmic extensions of pulpal neurons and odontoblasts. Situated between the enamel and dentin layers, the dentin-enamel junction (8) plays an important role in inhibiting crack propagation from enamel into dentin. This function stems from its complex, collagenous structure and biomaterial properties that are different from either dentin or enamel. Molecular structural differences in both mineral and organic matrix across the DEJ zone have been investigated by a two-dimensional confocal Raman micro spectroscopic mapping/imaging technique (9), by micro hardness (10, 11) and toughness (12), auto-fluorescence scanning (13), by FTIR imaging (14), and phosphate content by Raman spectroscopy (11). These results bolster the view, based on human and bovine teeth (9–14), that the thickness of the DEJ is functionally greater than the 2 microns visible from microscopy. However, there appears to be a difference in the estimated thickness ranging from ~100 microns to 4.7 microns with micro hardness. Second, a review of Raman quantitation of phosphate data published by Gallagher et al. (10) reveals a biphasic curve describing the variation in dentin, DEJ, and enamel. This data indicates that the amount of mineral gradually increases moving away from the DEJ up to an additional 10 microns.

Several groups have investigated how experimentally induced cracks propagate in the cuspal enamel and through the DEJ (15–17). The fractography revealed that the deviation of the crack path involved an area of enamel adjacent to the DEJ which was approximately 50–150 microns wide and displayed altered material properties. Collagen bundles with diameters of 80–120 nm which are oriented parallel to the DEJ zone, intertwine with dentin collagen fibrils, and penetrate 2–10 μm into the enamel (18) also likely play a significant role in resisting crack propagation from the enamel into the dentin layer. This reflects the fact that in the intact tooth multiple full thickness cracks commonly found in enamel do not typically result in catastrophic failure via crack extension into the dentin (13,14).

Gallagher et al.(13) used a 351-nm laser excitation source to perform auto fluorescence microscopy of dentin, enamel, and the DEJ to obtain information regarding their morphology and spectral characteristics. The emission spectra of these calcified dental tissues were different from one another, enabling the DEJ to be imaged and dimensions estimated. The DEJ displayed sharp and clearly delineated borders at both its enamel and dentin margins. The dentinal tubules and the enamel prisms appeared to terminate abruptly at the DEJ. The average median DEJ width was 10 microns, ranging from 7 to 15 microns, and it did not appear to depend on intra-tooth position. Depending upon which method is

[2]**Abbreviations**: MMP-20, matrix metalloproteinase-20 or enamelysin; DEJ, dentin-enamel junction; SEM, scanning electron microscopy; E, enamel; OM, organic matrix; D, dentin; IM, interphase matrix; PSh, prism-like sheaths; PS, prism-like scallops; Et, etched; NEt, non-etched; Et/B, etched and bleached; PBS, phosphate buffered saline; BSE, backscattered electron; HMDS, hexamethyldisilazane; CPD, critical point drying; ANOVA, analysis of variance; and EDTA, ethylene diamine tetracetic acid.

used, the thickness of the DEJ is estimated to be a graduated transitional region of 5 and 150 microns in width—distinctly broader than the 2 micron thick sharp morphological interface evident by optical microscopy. Thus, the DEJ can be appropriately defined as an interphase region of functionally graded properties intermediate between those of bulk phase enamel and dentin. These findings suggest that the functional properties of the DEJ extend beyond the interfacial boundary visible microscopically, however, it is unclear what the structural explanation is for these functional effects.

There is a long history of using scanning electron microscopy to investigate enamel structure. The first work (19) was carried out even before the introduction of commercial instruments and was performed on a prototype SEM microscope. Soon after the introduction of commercial instruments, numerous papers appeared describing the ultrastructure of etched enamel (20, 21). Etching of enamel is needed for both clinical reasons (22) and for revealing ultrastructural details of the enamel layer. Therefore, enamel etching is now a widely accepted technique in dental research, particularly in combination with SEM, and a number of papers containing SEM micrographs of etched enamel have been published (23–26). Nevertheless, none of these previous studies observed an organic matrix in enamel from mature healthy human teeth despite the fact that Tichenor and Taher (27) and Taher et al. (28) attempted to infiltrate de-proteinized human enamel with resin for the purpose of observing resin casts of the etched matrix. Resin infiltration was apparently unsuccessful because the micrographs of etched embedded enamel did not differ from those of published images of non-embedded enamel.

Since the enamel region closest to the optically thin DEJ is less mineralized and softer than bulk phase enamel, we speculate this is due to a higher protein content in the latter. However, little proof exists to support this rationale, nor evidence as to which protein(s) may be enriched in this region. We present results of a combined SEM and Raman spectroscopic approach on etched and non-etched full thickness human enamel sections which provides direct evidence for an organic protein containing layer extending ~100–400 μm away from the DEJ into the cuspal enamel. The appearance of this layer in SEM is distinctly different than that of enamel “tufts” (29). Since its limits resemble the DEJ interphase region defined functionally, we hypothesize that this organic layer may be responsible in part for the increased toughness and inhibition of crack propagation through the dentin-enamel junction.

MATERIALS AND METHODS

Source of human teeth

Teeth are de-identified and were collected according to protocol #03-06e approved by the University of Missouri-Kansas City Adult Health Sciences Institutional review board.

Specimen processing

Ten non-carious human third molars from different individuals were used in the study. The extracted teeth were stored from 3 days to 2 months at 4°C in 0.9% phosphate buffered saline with 0.002% sodium azide prior to processing. After removal of the roots, the crowns were sectioned bucco-lingually with a low speed diamond saw (Buehler Ltd., Lake Bluff, IL) to obtain 1.5 mm thick slices. Some of the slices were pre-fixed for 3 or 6 days in 2.5 % (w/v) glutaraldehyde in sodium cacodylate buffer (pH 7.4) before etching. Slices were fractured in two halves and immediately etched with either 4% EDTA for 30, 60, or 90 min (15 specimens) or 37% phosphoric acid for 15 sec, 60 sec, or 4 min (15 specimens). All specimens, excepting those prepared in the “minimalist” way (see below), were fixed with glutaraldehyde after etching. In all, 30 specimens were used in the study. Some of the

specimens fixed in glutaraldehyde were subsequently post-fixed in 1% osmium tetroxide. Finally, specimens were dehydrated in a graded series of alcohol solutions. To remove alcohol, specimens were then either treated with hexamethyldisilazane or by critical point drying (CPD030, Leica Microsystems GmbH, Wetzlar, Germany).

Throughout specimen preparation, a number of steps were taken in order to better preserve the fragile organic matrix. For example, specimens were maintained wet with the same surface up. Second, etching was performed by submerging in etching agent. Third, liquids were replaced by careful pipetting. And fourth, use of stirrers, shakers, running water, brushes, sprayers, etc. was avoided during preparation steps. In addition, to further minimize the potential impact of specimen preparation procedure on the retention and visualization of the organic layer, eight sections from four teeth were prepared in a "minimalist" way, e.g., limited only to essential preparation steps of etching, rinsing and air drying, with no fixation and no controlled dehydration.

Scanning electron microscopy

For SEM observation, specimens were sputter-coated (SCD050, Leica Microsystems GmbH, Wetzlar, Germany) with Au-Pd alloy and observed with a Field-Emission SEM XL30 (FEI, Hillsboro, OR) at a 5 or 15 kV accelerating voltage. After the observation of the flat saw-cut surface, specimens were turned 90° and the fractured surface was observed. In contrast, specimens processed via the "minimalist" approach were first observed without coating at a 1 kV accelerating voltage. For comparison, some of the "minimalist" specimens after observation with SEM and/or after acquisition of Raman spectra were treated with 5% sodium hypochlorite (NaOCl) solution for 30 minutes (bleached) to remove the interphase organic matrix remaining on surfaces of specimens after dissolution of mineral during etching.

Backscattered scanning electron micrographs were obtained from a carbon coated "minimalist" specimen (90 sec in phosphoric acid) at 5, 10, 15, 20 and 25 kV accelerating voltage. For the same specimen, the difference in etching depth between enamel and dentin was measured as an elevation of the dentin above enamel by direct measurements (a total of 20) on the SEM monitor. BSE coefficients were calculated with a freeware Monte Carlo electron flight simulation program *Casino*, developed at the University of Sherbrooke (Canada) (http://www.gel.usherbrooke.ca/casino/index.html, accessed 06/12/11). The backscattered electron coefficient represents the fraction of primary beam electrons that were converted to backscattered electrons through specimen interaction. Coefficients for experimental specimens were compared to coefficients calculated for pure enamel and for enamel covered with a layer of organic matter (gelatin) with the thickness of 400, 600, 800, 1000, 1200 and 1400 nm.

Confocal Raman spectroscopy

Tooth sections derived from four separate teeth were treated in different ways as noted above (non-etched, etched, etched and bleached). A LabRam HR 800 Raman spectrometer system equipped with a confocal microscope (Olympus BX41), a piezoelectric XYZ stage with a minimum step width of 50 nm, an air-cooled CCD detector of 1024–256 pixels, and a He-Ne laser (632.8 nm) (HORIBA JOBIN YVON, Paris, France) was used to collect Raman spectra on tooth sections. Spectra were collected using the following settings: a 600 grating, a 400-μm confocal hole, and a 100-μm slit width. Before data collection, the spectrometer was calibrated using a Raman-shift-frequency protocol with silicon.

Raman spectra were acquired by focusing the laser beam through a 100× Olympus objective onto the specimens. Raman spectra were acquired from two separate regions in the cuspal

enamel: Inner (within 50 μm of the DEJ) and 400 μm away from DEJ. Duplicate repetitive spectral scans (with 60 s accumulation time each) were carried out at each site over a range from 50 to 4000 cm^{-1}. Five different sites were selected manually within each of these two regions and duplicate spectra were collected at each site. A representative spectrum for each of the two regions of each tooth was obtained by averaging individual spectral scans. Finally, a multi-points baseline adjustment with lines mode, smoothing, and normalization based on the phosphate peak at 960 cm^{-1} was run on all spectra. Peak areas were determined using a two point baseline method.

Statistical analysis

A two-factor ANOVA and Tukey's post hoc analyses (α=0.05) were used to compare the protein/mineral ratio (2931/430 cm^{-1}), based on peak areas, as a function of enamel location and treatment (non-etched, etched, etched and bleached).

RESULTS

Ultrastructural characterization of the DEJ interphase layer in minimally processed tooth sections

Quantitative preservation of the organic matrix layer was found to be optimal when a "minimalist" processing protocol was used, even if the protocol did not preserve the morphology of the layer. Under these conditions (see METHODS), the organic matrix layer appeared as a dark, rough-edged 100–400 micron wide band on the surface of enamel and adjacent to the DEJ (Fig. 1b). We have termed this band the interphase layer due to its similarity in size to the functionally defined layer which inhibits crack propagation (13–15) and because the appearance of the band is unlike that of enamel tufts. At a higher magnification (Fig. 1c), the matrix on these specimens is devoid of detailed structure and looks rather like a smear coating on the enamel rods. Importantly, the interphase layer could be easily removed by treatment of minimally processed specimens with sodium hypochlorite, revealing the underlying structure of enamel rod etched mineral (Fig. 1d).

Imaging of a minimally processed specimen with backscattered electrons demonstrated that while readily apparent at a lower accelerating voltage of 5 kV (Fig. 1e), the interphase layer matrix became transparent at higher voltages (Figs. 1f and g). On the same specimen, the enamel was etched 19.1 +/− 3.1 μm STD deeper than the adjacent dentin. The backscattered coefficient for enamel was calculated as 0.19, and for enamel with a presumptive 800 nm thick organic matrix layer as 0.06, 0.16 and 0.18 at 5 kV, 15 kV and 25 kV, respectively. Results of calculations obtained under other conditions were used for comparative analysis (not shown).

Ultrastructural characteristics of the interphase matrix

In order to investigate the ultrastructure of the interphase region, longitudinal thick sections of the third molar teeth were fractured as shown in Figure 1a to provide an irregular viewing plane devoid of smear layer. An organic matrix layer was observed in all specimens and on both the flat side and on the fracture side (Fig. 1a). Typically, the interphase organic matrix followed the shape of the enamel rods (Fig. 2a). At higher magnification, the interphase matrix appeared to resemble a fibrous mesh-like structure (Fig. 2b). Since hydroxyapatite and collagen represent prominent extracellular matrix constituents of the DEJ, we immediately asked whether the interphase matrix resembled either of these materials. However, as shown in Figures 2c and d, respectively, the shape and interconnectivity of etched hydroxyapatite crystals of enamel and the collagen network of etched dentin were noticeably different when viewed at a similar magnification.

As illustrated in Figure 3a, the shape of the interphase matrix was not restricted to the shape of the mineral rods. Rather, frequently it resembled an enclosure or covering for the rods (Fig. 3a) and, prior to etching, it was enclosed within the sheath regions of rods. Micrographs of a different specimen etched for a shorter period of time (15 s) illustrate the micro structural differences between the interphase matrix and mineral crystals. The mineral (asterisks, Figs. 3b and c) is visible within the sheaths and was not completely removed by the shorter etching step. While the specimens in Figures 3b and c were treated with osmium tetroxide and CPD, Figures 3d and e provide an interesting comparison of the differential effects of an alternative dehydration method, HMDS, without post-fixation with osmium tetroxide. First, lower and higher power views of HMDS treated specimens resemble the empty enamel rod coverings or sheaths observed in Figure 3a. However, compared to the former, the sheaths appear to have collapsed and lost their 3-diminensional detail. Second, the interphase layer is clearly evident after HMDS treatment, displays a scalloped interface with the bulk enamel phase, and appears to be of a uniform minimum thickness of ~200 μm (Fig. 3d). Greater detail of the scalloped interfacial region was obtained inadvertently with a CPD dried specimen where the CPD built-in stirrer was turned on (in contrast with the other specimens). Specifically, the scalloped region appears to have lost most of its matrix. However, thick strands remain which connect the bulk enamel phase to the tips of individual residual matrix scallops (Fig. 3f). An internal view of the eroded interphase matrix at this location revealed a microfibrillar network possibly made up of collagen bundles (Fig. 3g).

Confocal Raman spectroscopy analysis of the interphase matrix

Because our SEM studies of minimally processed molar tooth sections demonstrated the existence of a novel interphase matrix extending about 100–400 μm into the enamel phase, we sought to obtain confirmatory evidence for its existence, as well as for its organic character, using confocal Raman spectroscopy. Our differential approach was influenced by the earlier SEM results which showed the interphase organic matrix layer was exposed by removal of associated surface mineral (etching), was predominantly localized within enamel to within 100–400 μm of the DEJ, and was largely removed by a mild wash with bleach, which should not remove further mineral. Thus, we predicted that if Raman spectroscopy was able to detect a component within the interphase matrix layer, this signal should be enriched close to the DEJ, and, be increased upon etching but decreased upon bleaching.

Figure 4 presents a graphical comparison of spectra collected from two separate enamel regions designated “Inner” representing 50 μm away from the DEJ and “400 μm” representing bulk cuspal enamel at least 400 μm away from the DEJ. Figure 4A represents a full spectral scan illustrating the mineralized nature of the enamel as well as demonstrating the ability of the etching step to uncover characteristic spectral signals in the 1200 to 3100 cm^{-1} range. Consistent with SEM results presented earlier, the bleaching step largely removed the latter peaks (Fig. 4A). We have restricted our attention to the spectral region between 2500 and 3200 cm^{-1} because the C—H stretching signal at 2931 cm^{-1} correlated directly with predicted characteristics of the interphase matrix layer (Fig. 4B). In view of the small shoulder evident at 2877 cm^{-1}, we believe that the 2931 cm^{-1} peak is derived from protein. As illustrated in Figure 4B (Inner), the C—H stretching signal increased dramatically after etching of the tooth section (compare line NEt with line Et). Each spectral line is the average of five separate scans within the designated areas. Following removal of the etched interphase matrix layer with bleach, the 2931 cm^{-1} peak was substantially diminished [compare line Et/B with line Et, Fig. 4B (Inner)]. Similar findings were qualitatively observed with three other molar teeth (results not shown). In contrast, Raman scans of the bulk enamel more than 400 μm away from the DEJ were largely invariant after various treatments. As shown in Figure 4B (“400 μm”), the C—H stretching peak did not increase appreciably after etching or decrease after bleaching as predicted from SEM results.

In summary, the 2931 cm^{-1} C—H stretching peak represents a protein-derived Raman signal (1, 2) which reflects the presence of an organic interphase matrix layer also visible by SEM.

Table 1 presents protein to mineral ratios (2931 cm^{-1}/430 cm^{-1}) at two locations in cuspal enamel, Inner enamel (up to 50 μm from the DEJ) or f400 μm from the DEJ. This ratio was chosen for several reasons. The 2931 cm^{-1} peak, reflecting a C--H stretching vibration, was larger than other possible spectral signatures for protein, e.g., amide I (1665 cm^{-1}), and the size of the 430 cm^{-1} peak associated with hydroxyapatite was more comparable to the 2931 cm^{-1} signal than that at 961 cm^{-1} (Fig. 4). Interestingly, the shoulder noted at 2877 cm^{-1} (Fig. 4B), which could represent CH_2 stretching vibrations of saturated acyl chains, may indicate the presence of triglycerides or phospholipids in the interphase matrix in addition to protein. Based on ANOVA and post hoc analyses, protein/mineral ratios were significantly higher ($p<0.05$) within Inner enamel near the DEJ across treatment groups (non-etched, etched, etched and bleached). In terms of treatment effects, within each location, non-etched enamel exhibited significantly lower ($p<0.05$) protein/mineral ratios as compared to the etched (de-mineralized) enamel. However, following subsequent bleach treatment of the etched surface (Et/B), the protein/mineral ratio was significantly lower ($p<0.05$) in enamel near the DEJ, while there was no significant change ($p >0.05$) in the protein/mineral ratio in enamel 400 μm from the DEJ.

DISCUSSION

The evidence presented in this paper support the following statements. First, SEM analyses revealed that enamel contains an interphase extracellular matrix layer located immediately adjacent and contiguous with the DEJ. The interphase layer, which shares some physical characteristics with enamel sheaths, displays a scalloped interface with the bulk enamel phase and extends at least 100–400 μm away from the DEJ. The appearance of the interphase matrix was readily distinguished from that of enamel tufts. Partial disruption of the layer revealed an interior collagenous fibrillar network. Second, confocal Raman spectral scans confirmed that the interphase matrix layer identified in SEM studies was enriched in a protein derived C—H stretching signal centered at 2931 cm^{-1}. This identification was based on a strict correlation between SEM and Raman results which demonstrated that both signals were exposed by etching and both were removed by bleaching, while both signals were also preferentially enriched within 100–400 μm of the DEJ. Third, these results provide physical evidence for the existence of a previously unappreciated organic matrix layer within enamel. Based on similarities in size and location, we believe the interphase matrix layer characterized here is the same as that functionally defined in crack propagation studies (15–17) and identified in nanoindentation studies (30). In summary, we propose the interphase matrix layer is an extracellular network that, in addition to the 2 micron wide DEJ, biomechanically stabilizes the interface between the dissimilar enamel and dentin phases.

The interphase matrix layer was found on both cut and fractured surfaces of all specimens used in the study. Its presence on the fractured surfaces ensures that it was not created by a smear layer. Confirmation that the observed matrix is protein-based is drawn from three observations. First, it can be removed by sodium hypochlorite, like the organic layer on the top of etched dentin (Fig. 3c). Second, in BSE micrographs, the interphase matrix layer has the same level of brightness as the organic layer on the top of etched dentin, indicating the two materials possess a similar mean atomic number. Third, Raman spectral scans detected a C—H stretch signal at 2931 cm^{-1} which is characteristic of C—H, CH_2, CH_3 groups in tissue proteins (30–32). This peak correlated directly with the presence or absence of the interphase layer during etching to expose it and bleaching to remove it. Interestingly, He and Swain (30) also showed that the increased protein content in the inner enamel layer

correlated with reduced hardness within 200 microns of the DEJ. Gallager et al.(11) showed that the C--H stretch signal (~2931 cm^{-1}) was present in dentin but not in enamel. However, we believe their inability to detect the 2931 cm^{-1} peak in enamel may have been due to its removal during ultrasonic cleaning steps.

The interphase matrix was not spread throughout the enamel, but created a layer 100–400 μm wide adjacent and contiguous with the DEJ. It is noteworthy that a number of investigators have observed changes in the chemical and mechanical properties of enamel close to the DEJ. For example, Meredith et al. (33) and Jeng et al. (34) showed that micro- and nanohardness decreased progressively towards the DEJ, whereas the content of organic matter in the enamel layer also increased close to the DEJ (30, 35). Functionally, several groups have also investigated if experimentally induced cracks in the cuspal enamel propagate through the DEJ (15–17). The fractography revealed that the deviation of the crack path involved an area which was approximately 50–150 μm wide in contrast to the DEJ thickness observed by optical microscopy. We propose that the interphase matrix layer serves to biomechanically stabilize the interface between the enamel and dentin-enamel junction.

Despite a long history of SEM studies of etched enamel, there have been no other confirmed observations of organic matrix in healthy adult teeth. We speculate this could be due to the extreme fragility of the matrix or to the use in the past of harsher specimen handling methods. For example, etching agent was applied with a minisponge (36); specimens were dried with compressed air after etching (37); specimens were rinsed with continuous agitation (38) or with water spray (39). We reason that all or most of the interphase matrix would be lost during such treatments and remnants could easily be treated as artifacts.

In contrast, the interphase layer was reproducibly imaged with SEM through use of a “minimalist” approach. Most often the interphase matrix was observed as a mesh-like structure that coincided with the sheath regions of enamel rods. Organic matrix was observed earlier (albeit as a more solid structure) primarily in regions of enamel that was highly hypomineralized due to fluorosis (40). Transmission electron microscopy revealed that mineral rods of highly hypomineralized enamel are separated by continuous mineral-free spaces, which were probably filled with organic matter (40, 41). Similar sheath-like regions in sound and healthy enamel contain only small mineral-free pores (41); these pores appear analogous to cross sections of the 3-D mesh structure of interphase matrix seen in Fig. 1d. Fagrell et al. (42) also observed enamel prisms in etched hypomineralized enamel covered by a structure-less layer. Similar to our “minimalist” specimen preparation, no attempt was made by these authors to preserve the structure of the layer via fixation or dehydration. However, it is not clear whether the character and amount of previously observed organic layers was not affected by the underlying pathology. For example, is removal of the enamel protein matrix, a prerequisite for completion of mineralization (43), delayed in hypomineralized teeth leading to an increased retention in residual enamel sheath proteins? If true, the organic layer in enamel from hypomineralized teeth is not representative of the situation in fully mineralized teeth like those examined here.

Evaluation of the interphase matrix layer in BSE as a function of accelerating voltage was performed in order to estimate its thickness. Depth of generation of BSE is much larger than that for secondary electrons and increases with an increase in accelerating voltage (44). When the whole depth of generation resides inside of the organic layer, the layer on the micrograph appears dark (co-efficient 0.06 at 5 kV, Fig. 3d). When depth of generation of BSE became bigger than the layer, the layer became semi-transparent and the underlying bright enamel becomes visible (coefficient 0.16 at 15 kV, Fig. 3e). When depth of generation was enlarged even further (co-efficient 0.18 at 25 kV, Fig. 3f), the interphase

layer became practically invisible since its co-efficient was similar to that for naked enamel alone (co-efficient 0.19, not shown). Comparison of calculated depth of generation of BSE with resultant specimen images provides a rough estimate of the thickness of the interphase matrix layer as 800 nm. The real depth of enamel etching was not measured, but a difference of 19.1 μm in the etching of enamel and dentin serves as a minimal estimate. Therefore, an 800 nm compacted organic layer would comprise 4% of the total volume of enamel dissolved by etching. This value is twice that accepted in the literature for the protein concentration in enamel (45), but it may reflect the fact that inner enamel is enriched in proteins.

Our results raise the question as to the source of the organic enamel matrix adjacent to the DEJ. While a definitive proof is outside the scope of this work, we speculate that the interphase matrix is a residual product of tooth development. Our rationale is based upon the similarities in appearance between the interphase layer and enamel sheaths. While sheath structures within bulk enamel are subject to degradation during the maturation stage of enamelogenesis by kallikrein-4 (46) and have been difficult to detect (47), biomaterials testing results have long indicated that prism sheath structures survive into adulthood (48–51). For example, Ge et al. (52), found the nanohardness and elastic modulus of the sheaths were 73.6% and 52.7% lower than those of the prisms in un-erupted third molars, respectively. The intraprismatic organic matrix in developing teeth is composed of relatively thin dense lines which are parallel to the long axes of the prisms within which they are located (53). Their appearance in longitudinal, oblique and cross sectional prism profiles indicates that it is organized into tubular sheaths which are oriented with their long axes parallel to the long axes of the prisms in which they are located. A predominant feature of the walls of the tubular sheaths is that of continuous sheets composed of filaments arranged in a basket weave fashion (53). Based on similarities in appearance and location, we propose that the interphase enamel layer characterized here in un-erupted third molars is comprised of residual prism sheaths.

Acknowledgments

We wish to thank Rachel Reed, Sarah McDonald, and Mrs. Nichole T. Huffman for their excellent technical assistance.

REFERENCES

1. Ryu OH, Fincham AG, Hu CC, Zhang C, Qian Q, Bartlett JD, et al. Characterization of recombinant pig enamelysin activity and cleavage of recombinant pig and mouse amelogenins. J Dent Res. 1999; 78(3):743–750. [PubMed: 10096449]
2. Llano E, Pendas AM, Knauper V, Sorsa T, Salo T, Salido E, et al. Identification and structural and functional characterization of human enamelysin (MMP-20). Biochemistry. 1997; 36(49):15101–15108. [PubMed: 9398237]
3. Simmer JP, Hu JC. Expression, structure, and function of enamel proteinases. Connect Tissue Res. 2002; 43(2–3):441–449. [PubMed: 12489196]
4. Paine ML, Zhu DH, Luo W, Bringas P Jr, Goldberg M, White SN, et al. Enamel biomineralization defects result from alterations to amelogenin self-assembly. J Struct Biol. 2000; 132(3):191–200. [PubMed: 11243888]
5. Paine ML, Zhu DH, Luo W, Snead ML. Overexpression of TRAP in the enamel matrix does not alter the enamel structural hierarchy. Cells Tissues Organs. 2004; 176(1–3):7–16. [PubMed: 14745231]
6. Smith CE, Hu Y, Richardson AS, Bartlett JD, Hu JC, Simmer JP. Relationships between protein and mineral during enamel development in normal and genetically altered mice. Eur J Oral Sci. 2011; 119(Suppl 1):125–135. [PubMed: 22243238]

7. Ten Cate, AR., editor. Oral histology: development, structure, and function. 5th Edition. Mosby, Inc.; St. Louis: 1998.
8. Walker, MP.; Fricke, BA. Dentin-Enamel Junction of Human Teeth. In: Metin, Akay, editor. Wiley Encyclopedia of Biomedical Engineering. John Wiley & Sons, Inc.; Hoboken, NJ: 2006.
9. Xu C, Yao X, Walker MP, Wang Y. Chemical/molecular structure of the dentin-enamel junction is dependent on the intratooth location. Calcif Tissue Int. 2009; 84(3):221–228. [PubMed: 19152060]
10. Marshall GW Jr, Balooch M, Gallagher RR, Gansky SA, Marshall SJ. Mechanical properties of the dentinoenamel junction: AFM studies of nanohardness, elastic modulus, and fracture. J Biomed Mater Res. 2001; 54(1):87–95. [PubMed: 11077406]
11. Gallagher RR, Balooch M, Balooch G, Wilson RS, Marshall SJ, Marshall GW. Coupled Nanomechanical and Raman Microspectroscopic Investigation of Human Third Molar DEJ. J Dent Biomech. 2010
12. Imbeni V, Kruzic JJ, Marshall GW, Marshall SJ, Ritchie RO. The dentin-enamel junction and the fracture of human teeth. Nat Mater. 2005; 4(3):229–232. [PubMed: 15711554]
13. Gallagher RR, Demos SG, Balooch M, Marshall GW Jr, Marshall SJ. Optical spectroscopy and imaging of the dentin-enamel junction in human third molars. J Biomed Mater Res A. 2003; 64(2): 372–377. [PubMed: 12522825]
14. Verdelis K, Crenshaw MA, Paschalis EP, Doty S, Atti E, Boskey AL. Spectroscopic imaging of mineral maturation in bovine dentin. J Dent Res. 2003; 82(9):697–702. [PubMed: 12939353]
15. Lin CP, Douglas WH. Structure-property relations and crack resistance at the bovine dentin-enamel junction. J Dent Res. 1994; 73(5):1072–1078. [PubMed: 8006234]
16. Dong XD, Ruse ND. Fatigue crack propagation path across the dentinoenamel junction complex in human teeth. J Biomed Mater Res A. 2003; 66(1):103–109. [PubMed: 12833436]
17. Bechtle S, Habelitz S, Klocke A, Fett T, Schneider GA. The fracture behaviour of dental enamel. Biomaterials. 31(2):375–384. [PubMed: 19793611]
18. Lin CP, Douglas WH, Erlandsen SL. Scanning electron microscopy of type I collagen at the dentin-enamel junction of human teeth. J Histochem Cytochem. 1993; 41(3):381–388. [PubMed: 8429200]
19. Boyde A, Stewart AD. Scanning electron microscopy of the surface of developing mammalian dental enamel. Nature. 1963; 198:1102–1103. [PubMed: 14014703]
20. Poole DF, Johnson NW. The effects of different demineralizing agents on human enamel surfaces studied by scanning electron microscopy. Arch Oral Biol. 1967; 12(12):1621–1634. [PubMed: 4966190]
21. Hoffman S, McEwan WS, Drew CM. Scanning electron microscopy of dental enamel. J Dent Res. 1968; 47(5):842. [PubMed: 5248932]
22. Buonocore MG. A simple method of increasing the adhesion of acrylic filling materials to enamel surfaces. J Dent Res. 1955; 34(6):849–853. [PubMed: 13271655]
23. Nichol T, Judd G, Ansell GS. Two-stage model for human enamel demineralization as determined by scanning electron microscope analysis. J Dent Res. 1973; 52(3):487–493. [PubMed: 4205148]
24. Lindau BM, Dietz W, Hoyer I, Lundgren T, Storhaug K, Noren JG. Morphology of dental enamel and dentine-enamel junction in osteogenesis imperfecta. Int J Paediatr Dent. 1999; 9(1):13–21. [PubMed: 10336712]
25. He B, Huang S, Zhang C, Jing J, Hao Y, Xiao L, et al. Mineral densities and elemental content in different layers of healthy human enamel with varying teeth age. Arch Oral Biol. 56(10):997–1004. [PubMed: 21411061]
26. Baharav H, Cardash HS, Helft M, Langsam J. The continuous brushing acid-etch technique. J Prosthet Dent. 1987; 57(2):147–149. [PubMed: 3550049]
27. Tichenor BL, Taher SM. Fibrous nature of the organic matrix of mature human enamel as studied by scanning electron microscopy using a replication technique. Trans Kans Acad Sci. 1983; 86(4): 144–148. [PubMed: 6419430]
28. Taher M, Aziz SM, Younis MN, Attia MA. Hassanein el S. A qualitative and quantitative study to assess the effect of different acid etching solutions on human enamel surface. I. Egypt Dent J. 1976; 22(2):1–18. [PubMed: 801870]

29. Amizuka N, Uchida T, Fukae M, Yamada M, Ozawa H. Ultrastructural and immunocytochemical studies of enamel tufts in human permanent teeth. Arch Histol Cytol. 1992; 55(2):179–190. [PubMed: 1497948]
30. He LH, Swain MV. Enamel--a functionally graded natural coating. J Dent. 2009; 37(8):596–603. [PubMed: 19406550]
31. Penel G, Delfosse C, Descamps M, Leroy G. Composition of bone and apatitic biomaterials as revealed by intravital Raman microspectroscopy. Bone. 2005; 36(5):893–901. [PubMed: 15814305]
32. Saar BG, Freudiger CW, Reichman J, Stanley CM, Holtom GR, Xie XS. Video-rate molecular imaging in vivo with stimulated Raman scattering. Science. 330(6009):1368–1370. [PubMed: 21127249]
33. Meredith N, Sherriff M, Setchell DJ, Swanson SA. Measurement of the microhardness and Young's modulus of human enamel and dentine using an indentation technique. Arch Oral Biol. 1996; 41(6):539–545. [PubMed: 8937644]
34. Jeng YR, Lin TT, Hsu HM, Chang HJ, Shieh DB. Human enamel rod presents anisotropic nanotribological properties. J Mech Behav Biomed Mater. 4(4):515–522. [PubMed: 21396600]
35. Weatherell, JAaR. C.S. The inorganic composition of teeth. In: Zipkin, I., editor. Biological Mineralization. Wiley Interscience; New York: 1973. p. 43-74.
36. Fjeld M, Ogaard B. Scanning electron microscopic evaluation of enamel surfaces exposed to 3 orthodontic bonding systems. Am J Orthod Dentofacial Orthop. 2006; 130(5):575–581. [PubMed: 17110254]
37. Goes MF, Sinhoreti MA, Consani S, Silva MA. Morphological effect of the type, concentration and etching time of acid solutions on enamel and dentin surfaces. Braz Dent J. 1998; 9(1):3–10. [PubMed: 9835798]
38. Hoffman S, Mc Ewan WS, Drew CM. Scanning electron microscope studies of EDTA-treated enamel. J Dent Res. 1969; 48(6):1234–1242. [PubMed: 4982901]
39. Shinohara MS, de Oliveira MT, Di Hipolito V, Giannini M, de Goes MF. SEM analysis of the acid-etched enamel patterns promoted by acidic monomers and phosphoric acids. J Appl Oral Sci. 2006; 14(6):427–435. [PubMed: 19089243]
40. Ekstrand, K.; Fejerskov, O.; Silverstone, LM. Fluoride in Dentistry. Munksgaard; Copenhagen: 1988.
41. Xie ZH, Mahoney EK, Kilpatrick NM, Swain MV, Hoffman M. On the structure-property relationship of sound and hypomineralized enamel. Acta Biomater. 2007; 3(6):865–872. [PubMed: 17638598]
42. Fagrell TG, Dietz W, Jalevik B, Noren JG. Chemical, mechanical and morphological properties of hypomineralized enamel of permanent first molars. Acta Odontol Scand. 68(4):215–222. [PubMed: 20392131]
43. Overall CM, Limeback H. Identification and characterization of enamel proteinases isolated from developing enamel. Amelogeninolytic serine proteinases are associated with enamel maturation in pig. Biochem J. 1988; 256(3):965–972. [PubMed: 3223966]
44. Goldstein, JNDE.; Joy, DC.; Lyman, CE.; Echlin, P.; Lifshin, E.; Sawyer, L.; Micheal, JR. Scanning electron microscopy and x-ray microanalysis. Third Edition. Springer Publishing Co.; 2003.
45. Van Rensburg, B. Oral Biology. 1st Edition. Berlin Quintessence Publishing; 1995.
46. Lu Y, Papagerakis P, Yamakoshi Y, Hu JC, Bartlett JD, Simmer JP. Functions of KLK4 and MMP-20 in dental enamel formation. Biol Chem. 2008; 389(6):695–700. [PubMed: 18627287]
47. Warshawsky H. Organization of crystals in enamel. Anat Rec. 1989; 224(2):242–262. [PubMed: 2672889]
48. Waters NE. Some mechanical and physical properties of teeth. Symp Soc Exp Biol. 1980; 34:99–135. [PubMed: 7020144]
49. He LH, Fujisawa N, Swain MV. Elastic modulus and stress-strain response of human enamel by nano-indentation. Biomaterials. 2006; 27(24):4388–4398. [PubMed: 16644007]
50. Haines DJ. Physical properties of human tooth enamel and enamel sheath material under load. J Biomech. 1968; 1(2):117–125. [PubMed: 16329299]

51. Spears IR. A three-dimensional finite element model of prismatic enamel: a re-appraisal of the data on the Young's modulus of enamel. J Dent Res. 1997; 76(10):1690–1697. [PubMed: 9326902]

52. Ge J, Cui FZ, Wang XM, Feng HL. Property variations in the prism and the organic sheath within enamel by nanoindentation. Biomaterials. 2005; 26(16):3333–3339. [PubMed: 15603829]

53. Travis DF, Glimcher MJ. The Structure and Organization of, and the Relationship between the Organic Matrix and the Inorganic Crystals of Embryonic Bovine Enamel. J Cell Biol. 1964; 23:447–497. [PubMed: 14245432]

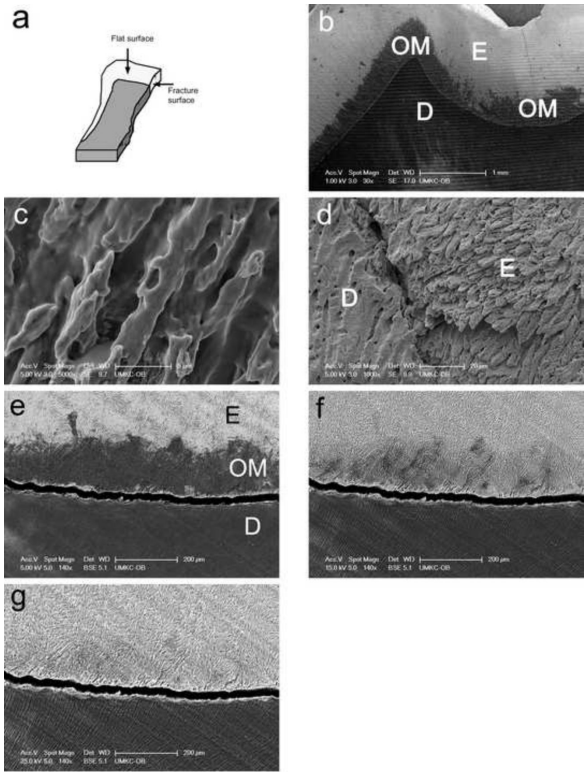

Fig. 1. Identification of interphase organic matrix layer within enamel of mature teeth near the dentin enamel junction

a, a diagram illustrating shape and orientation of tooth sections used in this study.

b, specimen processed according to “minimalist” protocol and observed without coating at 1 kV accelerating voltage.

c, the microstructure of organic matrix of the “minimalist” specimen, observed on Au-Pd coated specimen.

d, the microstructure of underlying enamel rods after removing of organic matrix from “minimalist” specimen with sodium hypochlorite.

e, specimen processed according to “minimalist” protocol and backscattered electron image collected at 5 kV.

f, specimen processed according to “minimalist” protocol and backscattered electron image collected at 15 kV.

g, specimen processed according to “minimalist” protocol and backscattered electron image collected at 25 kV.

Individual bars refer to microscopic scales for each image.

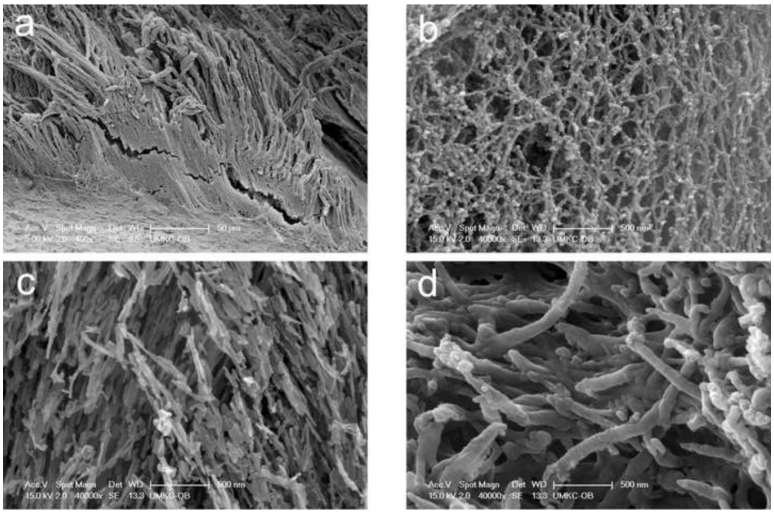

Fig. 2. Ultrastructural characteristics of the enamel interphase matrix layer

a, appearance of organic enamel matrix at fracture surface prefixed for 6 days, etched in EDTA for 90 min, fixed in glutaraldehyde, post fixed in OsO_4 and subjected to critical point drying.

b, higher magnification view of enamel organic matrix at fracture surface after specimen prefixation for 6 days, etching in phosphoric acid for 45 sec, fixing in glutaraldehyde, and critical point drying.

c, enamel hydroxyapatite crystals after etching in phosphoric acid for 45 sec, fixing in glutaraldehyde and drying (same magnification and same specimen as in 1B above).

d, collagen network of dentin (same magnification, processing, and specimen as in 1C above) (bar=500 nm).

Individual bars refer to microscopic scales for each image.

KEY: **E**, enamel; **OM**, organic matrix; **D**, dentin

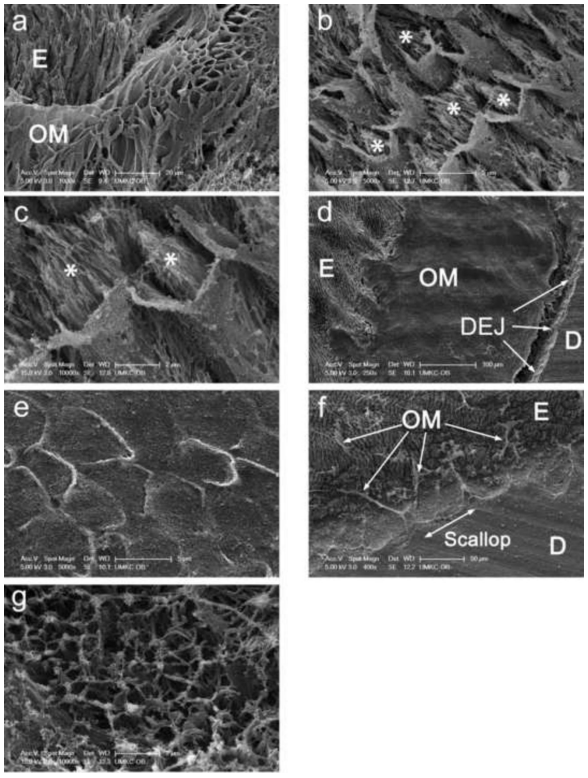

Fig. 3. Identification of sheath-like structures within the enamel interphase matrix

a, appearance of organic enamel matrix at flat surface of tooth section after etching in EDTA for 90 min, fixation in glutaraldehyde, post fixing in OsO_4 and critical point drying.

b, interphase matrix at fracture surface after prefixation for 3 days, etching in phosphoric acid for 15 sec, fixation in glutaraldehyde, post fixation in OsO_4, and critical point drying. Asterisks refer to mineral crystals within sheath-like structures.

c, higher magnification view of same specimen as in B. Asterisks refer to mineral crystals within sheath-like structures.

d, appearance of region near the dentin-enamel junction at flat surface after prefixation for 6 days, etching in EDTA for 60 min, fixation in glutaraldehyde, and dehydration with HMDS.

e, higher magnification view of same specimen as in D.

f, appearance of region at fracture surface after prefixation for 6 days, etching in EDTA for 30 min, fixation in glutaraldehyde, post fixation in osmium tetroxide and critical point drying with built in magnetic stirrer turned on (jagged edge of dentin-enamel junction readily visible, arrows).

g, higher magnification view of same specimen as in F (collagen bundles readily visible). Individual bars refer to microscopic scales for each image.

KEY: **E**, enamel; **OM**, organic matrix; **D**, dentin; **DEJ**, dentin-enamel junction

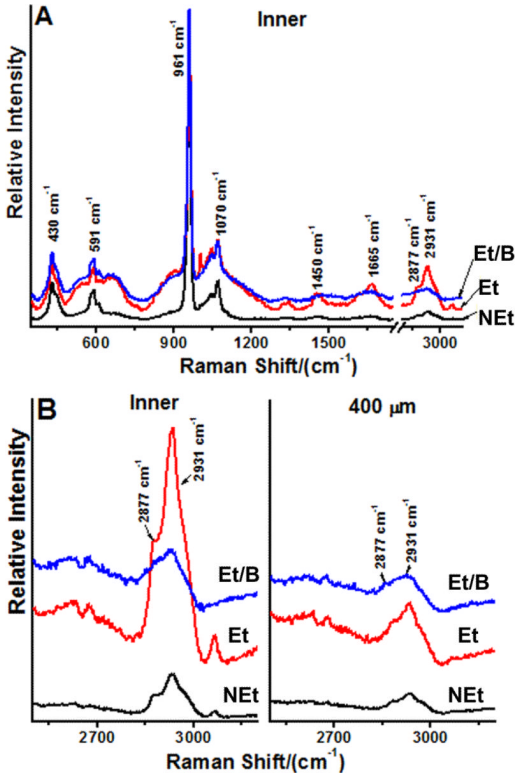

Fig. 4. Confocal Raman spectroscopic analysis of the enamel interphase matrix

Data shown are representative of scans of sectioned teeth from four different individuals. **A**, baseline corrected Raman spectra of enamel at a location 50 μm (Inner) from the dentin-enamel junction. Spectra were recorded before and after sequential etching and bleaching steps. Five separate scans were made at different sites for each condition and averaged to generate the spectra shown. A higher resolution view of the region of interest between 2500 and 3200 cm^{-1} is presented in **B**. **KEY**: **NEt**, non-etched; **Et**, etched; and, **Et/B**, etched and bleached.

B, baseline corrected Raman scans of a sectioned tooth at two different locations, near the dentin-enamel junction (Inner) and at least 400 μm away from the dentin-enamel junction (400 μm). Spectra were recorded at these locations before and after etching and bleaching steps. Five separate scans were made at each enamel location for each condition and averaged to generate the curves shown. **KEY**: **Inner**, enamel 50 μm from the dentin-enamel junction; **400 μm**, enamel at least 400 μm away from the dentin-enamel junction; **NEt**, non-etched; **Et**, etched; and, **Et/B**, etched and bleached.

Table 1

Average peak ratios of 2931 cm^{-1}/430 cm^{-1} before and after treatments

Enamel Location*	Ratio	NEt (Mean±SD)	Et (Mean± SD)	Et/B (Mean±SD)
400 μm**	2931/430	0.10±0.17^{aA}	0.23±0.17^{aB}	0.23±0.08^{aB}
Inner**	2931/430	0.34±0.23^{bB}	0.97±0.83^{bA}	0.37±0.09^{bB}

Footnotes:

Enamel locations: 400 μm from DEJ; Inner= 50 μm from DEJ

Treatments: NEt =non-etched; Et=etched; Et/B= etched, then bleached

Average peak ratios were obtained from measurements on four separate teeth

*The protein/mineral ratios are significantly higher in inner enamel as compared to enamel 400 microns from the DEJ across treatment groups (subsets indicated by small case letters).

**Within each enamel location, there are also significant differences in protein/mineral ratios among treatments (subsets indicated by capital letters).